Chemical Geology 617 (2023) 121274

Contents lists available at ScienceDirect

Chemical Geology

journal homepage: www.elsevier.com/locate/chemgeo

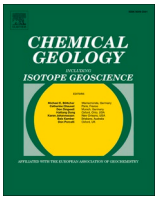

# Evaluating the biosignature potential of nitrogen concentrations in graphite and associated K-silicates

Eva E. Stüeken [a,*], Kristoffer Szilas [b], Vincent J. van Hinsberg [c]

[a] University of St Andrews, School of Earth & Environmental Sciences, Bute Building, Queen's Terrace, St Andrews, Fife KY16 9TS, United Kingdom
[b] Department of Geosciences and Natural Resource Management, University of Copenhagen, Øster Voldgade 10, 1350 Copenhagen K, Denmark
[c] GEOTOP Research Centre, Department of Earth & Planetary Sciences, McGill University, 3450 Rue University, Montréal, Québec H3A 0E8, Canada

ARTICLE INFO

Editor: Balz Kamber

*Keywords:*
Graphite
Eoarchean
Biosignatures
Nitrogen abundances

ABSTRACT

The oldest remnants of life on Earth from various localities in the Isua supracrustal belt in Greenland date back to >3.7 billion years ago (Ga). They are in the form of graphite, whose biogenicity is controversial. Previous studies used the presence and isotopic composition of nitrogen in graphite from along the Isua belt to argue both for and against biogenicity. To determine if the nitrogen chemistry of graphite can indeed serve as a biosignature, we investigated a hydrothermal graphite deposit from south-east Greenland (1.87–1.82 Ga). We found indications that molar C/N ratios of hydrothermal graphite may be similar to those of biogenic graphite from the Archean rock record, meaning that the nitrogen content of graphite is itself perhaps not diagnostic of ancient life, requiring caution in future studies. However, the hydrothermal graphite deposit also revealed unusually low N concentrations in associated silicates, despite a wide range of K concentrations up to 5 wt%. Using a thermodynamic model of nitrogen speciation in the presence of graphite, paired with previously published partition coefficients for ammonium in K-silicates, we show that abiotic process can explain these low N-concentrations of around 1 μg/g in potassic silicates. Higher concentrations of >10 μg/g, such as those found in graphitic metapelites from the Isua supcracrustal belt, would, however, require an unusually ammonium-rich fluid. Such an ammonium-rich fluid is most easily derived from the breakdown of biomass within sediments prior to graphitization. We therefore conclude that potassic silicates associated with graphite can serve as an indirect biosignature. Our approach supports previous inferences of life on Earth back to at least 3.7 Ga.

## 1. Introduction

Some of the oldest putative remnants of life on Earth are preserved in the form of graphite, i.e., crystalline solid carbon with a redox state of zero ($C^0$). Examples include a graphite inclusion in a 4.1 billion year old (Ga) zircon (Bell et al., 2015), graphitic metapelites in northern Labrador from 3.95 Ga (Tashiro et al., 2017) (but see Whitehouse et al., 2019 for a different assessment of the depositional age) and in the >3.7 Ga Isua supracrustal belt (Rosing, 1999; Ohtomo et al., 2014), as well as graphite inclusions within banded iron formation from Isua (Mojzsis et al., 1996) and from Akilia Island at 3.85 Ga (Mojzsis et al., 1996) (but see alternative evidence from Fedo and Whitehouse, 2002; Lepland et al., 2005). Graphite inclusions have also been reported from banded iron formations in the Nuvvuagittuq Supracrustal Belt (>3.75 Ga), but these were concluded to post-date peak metamorphism (Papineau et al., 2011). However, if any of these occurrences are indeed indigenous and syngenetic with the host rock, these findings would imply that life originated already during the Hadean and was possibly present during the time of heavy meteorite bombardment (Abramov and Mojzsis, 2009). The graphite that this evidence is based on is thought to have formed during metamorphism, as organic carbon that had originally been buried within marine sediments was subjected to elevated pressures and temperatures. Metamorphism is known to progressively remove functional groups, including most H, O, N, S and minor elements from the original biomass, while the remaining carbon is reorganised into graphite sheets (Hayes et al., 1983). Graphite would therefore be the expected remnant of early life in these geological settings. However, graphite can also form from non-biological C-sources (e.g., Huizenga, 2011). For example, carbonate and $CO_2$ may be reduced to $C^0$, and $CH_4$ may be oxidized to $C^0$ under appropriate redox and pressure-temperature conditions. Therefore, the mere presence of graphite alone is not sufficient evidence for life on the early Earth. This possibility

* Corresponding author.
*E-mail address:* ees4@st-andrews.ac.uk (E.E. Stüeken).

https://doi.org/10.1016/j.chemgeo.2022.121274
Received 12 August 2022; Received in revised form 25 November 2022; Accepted 18 December 2022
Available online 20 December 2022

has fuelled debates about the biogenicity of the earliest graphite occurrences in the rock record (van Zuilen et al., 2002; van Zuilen et al., 2005). Additional lines of evidence that have been used in support of a biological origin are the isotopic composition of the graphite (Mojzsis et al., 1996; Rosing, 1999; Ohtomo et al., 2014), in particular relative to co-occurring carbonate (Tashiro et al., 2017), as well as trace amounts of residual N, O and P within the graphite that could be relics of former biomolecules (Hassenkam et al., 2017). However, hydrothermal redox reactions that convert $CO_2$, CO and/or $CH_4$ to graphite can potentially mimic the isotopic composition that would be expected from biological metabolisms (Horita, 2001; Kueter et al., 2019), meaning that carbon isotopes alone are supportive but inconclusive evidence of biogenicity. Similarly, it is conceivable that abiological graphite incorporates impurities from the environment that it forms in. For example, van Zuilen et al. (2005) extracted nitrogen with an isotopic composition ($\delta^{15}N$) as low as −3.7 ‰ from graphite contained in metacarbonates and schists from Isua and proposed that this nitrogen was of abiotic origin, derived from local igneous rocks.

To further address if the nitrogen chemistry of graphite can be indicative of biogenicity, we investigated hydrothermal graphite deposits in the Tasiilaq area of south-east Greenland that is thought to have formed from redox conversions of fluid-derived $CO_2$ and/or $CH_4$ (Rosing-Schow et al., 2017). We study a suite of samples taken in the same field campaign by us from localities that overlap in characteristics. The formation temperature is estimated to be ca. 600 °C (Rosing-Schow et al., 2017). Hence, this graphite can serve as a natural laboratory to test if metasomatic graphite is indeed distinct in its nitrogen chemistry from biogenic graphite. We find that the graphite itself is likely not sufficiently distinct; however, the associated silicate rock is unusually depleted in nitrogen compared to graphite-bearing metasedimentary rocks from the Isua Supracrustal Belt, despite comparable levels of K, which has a similar ionic size and the same charge as ammonium ($NH_4^+$). We present new thermodynamic models to show that fluids without any biological source of nitrogen are relatively depleted in ammonium under conditions where graphite is thermodynamically stable, and therefore the ammonium content of K-silicate minerals (micas, feldspars) is very low. K-silicates associated with graphite may therefore serve as an indirect tool to gauge graphite biogenicity. This work builds upon previous studies that documented elevated levels of ammonium in micas and inferred a biological origin (Itihara and Suwa, 1985; Boyd, 2001), including metasedimentary rocks from Isua (Honma, 1996; Pinti et al., 2001; Papineau et al., 2005). Our new thermodynamic model provides quantitative support for this approach.

## 2. Geological setting

### 2.1. Regional geology

The Tasiilaq region of SE Greenland exposes the suture between the North Atlantic and Rae cratons, resulting from horizontal convergence and collision that culminated in the 1.9 Ga Nagssugtoqidian orogeny (Hall et al., 1989; Kalsbeek et al., 1993; Nutman et al., 2008; Kolb, 2014). The North Atlantic Craton in the area is represented by the Isertoq terrane, which acted as the overriding plate in the convergence, whereas the Kuummiut terrane and the Schweizerland terrane to the north of it are part of the Rae craton (Fig. 1). The basement in the area consists of amphibolite to granulite-facies Archaean to Palaeoproterozoic gneisses, dominated by orthogneisses of tonalite-trondhjemite-granodiorite (TTG) affinity with ages from 3.1 Ga to 2.7 Ga (Wright et al., 1973; Nutman and Friend, 1989; Kalsbeek et al., 1993; Nutman et al., 2008; Kolb, 2014; Kokfelt et al., 2016; Crotty et al., 2022). The polyphase TTG gneisses enclose abundant layers, lenses and pods of amphibolite, ultramafic rocks, and, locally, anorthosite. Intrusive relations are mostly obscured by deformation, but where visible generally suggest intrusion of TTGs into an earlier basement of amphibolite and diorite (Van Hinsberg and Poulsen, 2018; Crotty et al., 2022; Poulsen, 2022).

The basement is tectonically overlain by supracrustal belts, including the Kap Tycho Brahe Unit in the Isertoq terrane (Kolb, 2014; Poulsen, 2022), the Kuummiut and Helheim Units in the Kuummiut terrane

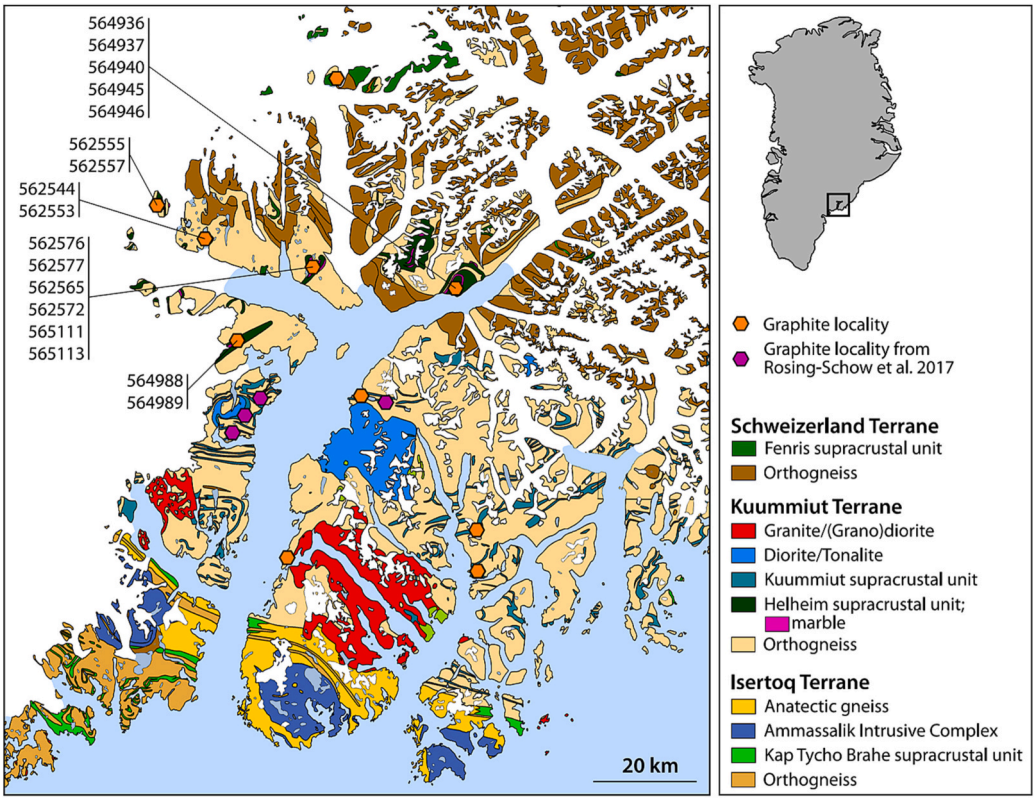


**Fig. 1.** Geological overview map of the study area (geology after Kolb et al. 2014 and Crotty et al., 2022, more detailed geological maps for the area are available from the Geological Survey of Denmark and Greenland). Sample localities (Table 1) are highlighted with orange symbols and those discussed by Rosing-Schow et al. (2017) in dark pink. K. = Kuummiut village, Tin. = Tiniteqilaaq village. (For interpretation of the references to colour in this figure legend, the reader is referred to the web version of this article.)

(Kolb, 2014; Crotty et al., 2022) and the Fenris Unit in Schweizerland (Crotty et al., 2022). The supracrustal belts contain a diversity of metasedimentary lithologies including metapelite, marble, calc-silicate rocks and quartzite, as well as volcanic or shallow intrusive magmatic rocks, predominantly metabasalts (Hall et al., 1989; Kolb, 2014; Crotty et al., 2022; Poulsen, 2022). These lithologies are thought to have been deposited in interconnected basins in volcanic arc and back-arc basin settings at ca. 2.0–2.2 Ga (Kalsbeek et al., 1993) (Crotty et al., 2022).

A diverse suite of igneous bodies intrudes the basement, including dunites and lherzolites, diorites, granites and tonalites (Kalsbeek et al., 1993; Kokfelt et al., 2016) (Kalsbeek, 1989; Nicoli et al., 2018; Poulsen, 2022). The Ammassalik Intrusive Complex (AIC, Fig. 1) is particularly prominent. The AIC intruded the northern margin of the Isertoq terrane in three pulses from 1910 Ma to 1870 Ma (Kalsbeek et al., 1993; Lebrun et al., 2018), and developed an extensive contact aureole with migmatisation (Kalsbeek et al., 1993). The large granite bodies in the Kuummiut and Isertoq terranes are post-orogenic (Kokfelt et al., 2016) and related to orogenic collapse (Kolb, 2014). They are associated with multiple generations of pegmatite sheets (Poulsen, 2022).

The basement records a multi-phase metamorphic history with an early amphibolite to granulite-facies metamorphism and migmatisation, (partially) overprinted by a predominantly amphibolite-facies metamorphic event related to the Nagssugtoqidian orogeny (Kalsbeek et al., 1993; Nutman et al., 2008; Kolb, 2014). Locally, eclogite-facies relics are found in the Kuummiut terrane, which document the subduction stage of collision (Nutman et al., 2008; Müller et al., 2018) Epidote-chlorite assemblages in veins and their host rocks represent late-stage greenschist facies retrogression.

### 2.2. Graphite

Graphite is found throughout the Kuummiut and Schweizerland terranes (Fig. 1). It occurs in marbles, calc-silicate rocks, amphibolites, orthogneisses and biotite-schists (Fig. 2), and locally in veins where it can be the dominant or even sole mineral. High graphite abundances are generally associated with hydrothermal alteration to form friable sericite schists that are easily recognizable in the field by distinct yellow-brown weathering (Fig. 2d). The graphite-rich occurrences appear to be related to a metasomatic event that introduced carbon, leading to strong alteration and abundant graphite along fluid pathways and a more diffuse introduction of graphite into lithologies more distal to these fluid channels. Graphite is also associated with shear zones, strike-slip faults and lithology contacts (e.g. Fig. 2a), which likely acted as preferential fluid channels, although remobilisation of graphite onto shear planes is also observed. Graphite occurs from idiomorphic, isolated grains to fine-grained masses (Fig. 3), generally parallel to the foliation of the rock, although it is also found as cross-cutting veins. Decimetre-wide massive graphite bands were reported by Rosing-Schow et al. (2017) in other parts of the Tasiilaq area.

The graphite reflects three stages in the history of its host rocks. Graphite inclusions in prograde growth-zoned garnet represent the first generation and indicate that graphite was present on the prograde path of the Fenris and Helheim unit meta-pelites (Fig. 3a,b). In addition to isolated idiomorphic graphite flakes, graphite is also found in enigmatic multi-mineralic inclusions in the garnet. Graphite inclusions are moreover found in clino-amphibole in meta-basalts from the Kuummiut Unit, where they occur together with relict prograde epidote inclusions. The


**Fig. 2.** Outcrop photographs of graphite occurrences in the field area: a. Graphite-bearing schist at the contact between amphibolite and meta-pelitic gneiss in the Fenris Unit; b. Marble and calc-silicate gneiss succession in the Kuummiut Unit at Cap Nuuk hosting disseminated graphite; c. Abundant graphite in sericite schist in Tiniteqilaaq village; d. Typical weathering of graphite-bearing sericite schist in the Helheim Unit with graphite being the grey phase above the hammer. Mineral abbreviations: gph = graphite, q = quartz.

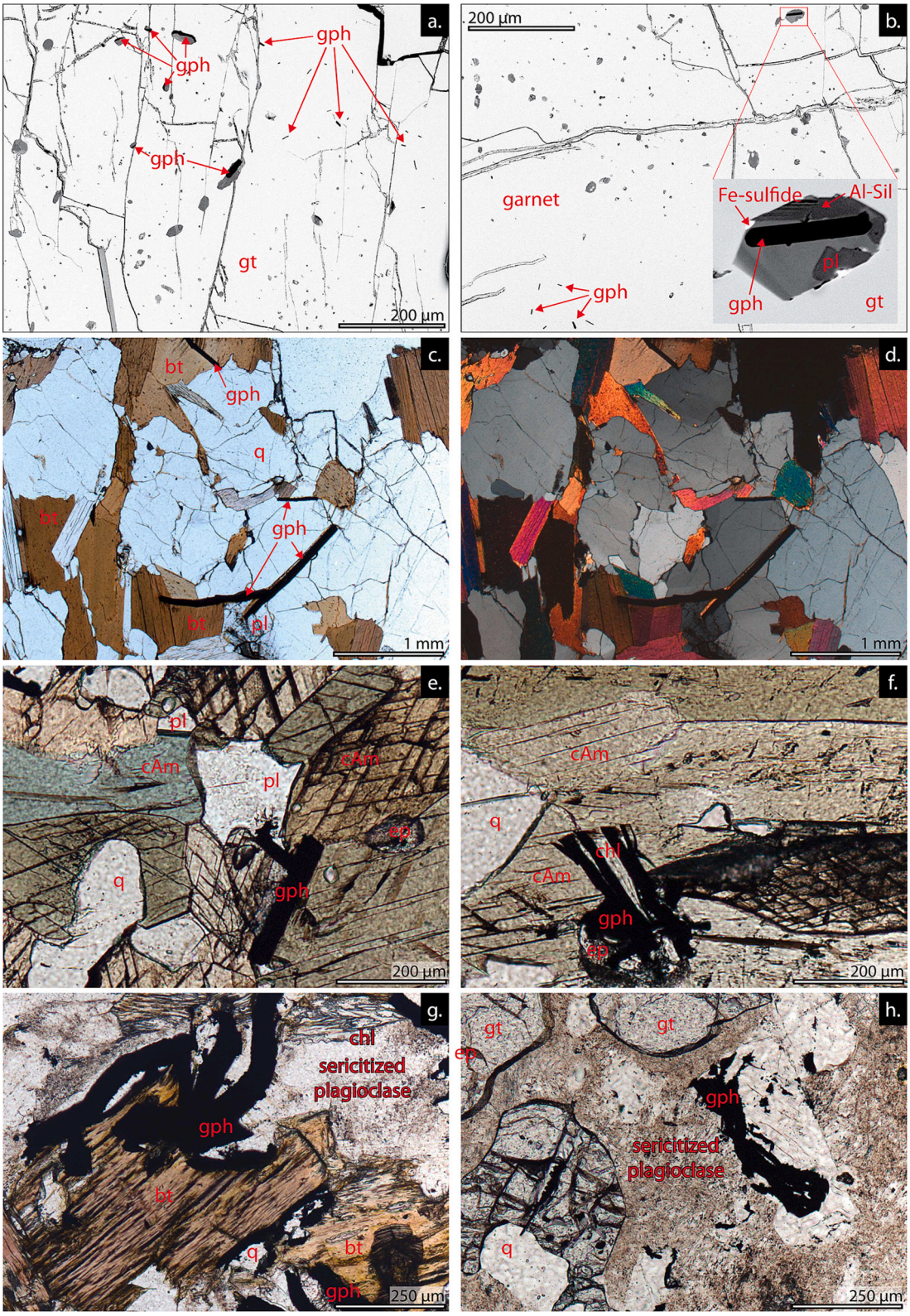


**Fig. 3.** Micrographs of typical graphite textures: a, b. BSE images of inclusions in prograde growth-zoned garnet in meta-pelite from the Fenris Unit (kya-zone). Graphite is found in isolated flakes and in multi-mineralic inclusions; c.d. PPL and XPL micrographs of meta-pelite from the Fenris Unit (sill-zone) with graphite intergrown with the peak metamorphic minerals; e. Graphite intergrowth with peak metamorphism and plagioclase in meta-basalt from the Kuumiut Unit; f. Graphite associated with retrograde chlorite and epidote in Kuummiut Unit meta-basalt; g. Irregular-shaped graphite associated with sericitization of plagioclase, retrogression of biotite, and appearance of chlorite; h. Late-stage graphite in gt-pl meta-sediment from the Kuummiut Unit. Mineral abbreviations: gph = graphite, bt = biotite, cAm = clino-amphibole, q = quartz, pl = plagioclase, ep = epidote, chl = chlorite, gt = garnet, Al-Sil = Al-silicate.

graphite inclusions are commonly aligned and preserve a relict prograde foliation direction.

A second type of graphite is intergrown with the upper-amphibolite facies peak metamorphic minerals in meta-basalts, meta-pelites, calc-silicate rocks, and marbles. These graphite grains are larger than those found as prograde relics. In the meta-pelites, they occur as large, idiomorphic grains, commonly on the basalt plane of biotite (Fig. 3c,d). In the meta-basalt, they are found on grain boundaries (Fig. 3e). In calc-silicate rocks and marbles, they occur as disseminated grains in between the carbonate phases. The graphite flakes are generally aligned to the peak metamorphic foliation.

The third type of graphite is metasomatic in origin and commonly associated with retrogression. This is by far the dominant type of graphite in the field area. It is distinct from that described earlier in being irregular in shape, with elongate grains bent and split, and the presence of clusters and masses of finer-grained graphite (Fig. 3f,g,h). Graphite abundances are higher than for either the prograde or peak metamorphic types, and graphite is found in a larger range of bulk rock compositions. In meta-basalts, we observe metasomatic graphite associated with actinolite + chlorite + epidote greenschist-facies retrogression (Fig. 3f), whereas in meta-sediments it occurs together with albitized and sericitized plagioclase, (partially) retrogressed biotite and introduction of chlorite (Fig. 3g,h). This type of occurrence corresponds to that described by Rosing-Schow et al. (2017), who additionally identified pumpellyite as an associated phase. However, these authors also describe an earlier, higher temperature metasomatic introduction of graphite associated with garnet and amphibole. We did not observe this stage among our sample suite. Although formed at higher grade conditions, this stage is regarded as post peak metamorphism (Rosing-Schow et al., 2017).

The main graphite occurrences in the Tasiilaq area probably formed from mixing (± cooling) of $CO_2$- and $CH_4$-bearing fluids either in two events at conditions of ca. 600 and 400 °C, respectively, or in a main event followed by later greenschist-facies remobilisation (Rosing-Schow et al., 2017). The ultimate source of the C is unknown. Marbles and carbonate-bearing calc-silicate rocks are presents in the area, and we observe prograde and peak-metamorphic graphite in meta-sediments and meta-basalts. However, neither appears to be a good C source. Primary graphite is present in textural equilibrium with the metamorphic silicate and carbonate phases in marbles and calc-silicate rocks, and the metasomatic graphite in these samples represents addition, not local remobilisation or a carbonate reduction reaction. Metamorphic graphite in the meta-basalts and meta-sediments is a minor constituent, and there is no evidence for its mobilisation. Indeed, it commonly acts as a nucleation surface for later metasomatic graphite. It would thus appear that the C is not locally sourced. Rosing-Schow et al. (2017) conclude, based on the strong $^{13}C$ isotopic depletion, that the source was biological, but this reservoir has yet to be identified in the area.

Metasomatic graphite is found throughout the Kuummiut and Schweizerland terranes, in diverse lithologies and mineral assemblages, and with a common, characteristic potassic alteration to sericite-graphite schists. This indicates that it represents a regional metasomatic event that must postdate thrusting of the Schweizerland terrane onto the Kuummiut terrane.

## 3. Analytical methods

Polished thin sections were prepared for representative samples of meta-basalt, meta-sediment, biotite schist, marble and calc-silicate rock with a focus on the supracrustals units of the Isertoq, Kuummiut, and Schweizerland terranes. These thin sections have been studied in optical and back-scattered electron imaging, and by Energy-Dispersive Spectrometry using a PhenomXL desktop SEM. The samples selected for C and N study are all dominated by graphite of metasomatic origin.

Hand samples were prepared for elemental and isotopic analyses following established protocols at the University of St Andrews (Stüeken et al., 2021). First, the rocks were hammered into sub-cm chips, which were rinsed sequentially within pre-combusted (500 °C) glass beakers with DI-water (18 MΩ $cm^{-1}$), methanol (reagent grade), 1 M HCl (reagent grade), and again DI-water. The chips were then dried in a closed oven at 70 °C. The dry chips were pulverized in an agate ball mill and stored in pre-combusted scintillation vials.

### 3.1. Carbon and nitrogen analyses

A ~ 0.5 g aliquot of each sample was decarbonated within pre-combusted glass centrifuge tubes, using ~10 ml of 2 M HCl at 70 °C overnight. The next day, the acid was decanted after centrifugation (700 rpm for 15 min) and a few drops of fresh acid were added to each sample to ensure that no further effervescence occurred and all carbonate had been removed. The acid was then washed out with three treatments of ~15 ml of DI-water, and the remaining powder was left to dry in the oven. The mass difference between the dry decarbonated powder and the initial untreated sample aliquot was used as a rough estimate of the total carbonate content. To further ensure that all carbonate had been completely removed and was not impacting the carbon isotope measurements, we later performed additional decarbonations with two treatments of 12 M HCl at 70 °C overnight. With the exception of one sample the measured difference in $\delta^{13}C$ was 1.8‰ or less (the average offset in absolute terms was 0.6‰), indicating that even the relatively high $\delta^{13}C$ values (see below) are not affected by residual carbonate contamination. The carbon data reported in Table 1 are for the sample aliquots treated with 12 M HCl.

From the decarbonated powder, small aliquots of each sample were weighed into tin capsules (8 mm × 5 mm) and analysed by flash combustion with an EA Isolink coupled via a ConFlo IV to a MAT253 IRMS (all Thermo Fisher). The EA was equipped with an oxidation column at 1020 °C, a reduction column at 650 °C and a water trap (± $CO_2$ trap, see below) at room temperature. The oxidation column was packed with $Cr_2O_3$ granules as oxidation aid and silvered cobaltous cobaltic oxide granules for removing sulfur from the gas stream. The reduction column was packed with Cu wire to convert $NO_x$ gases to $N_2$ and trap excess $O_2$ gas. The water trap was packed with magnesium perchlorate granules. For analyses of nitrogen content within the graphite, $CO_2$ was extracted from the gas stream by adding soda lime granules to the water trap, preceding the magnesium perchlorate. The purified gases were sent through a gas chromatography column that was ramped from 35 °C to 240 °C during each run to optimize the elution of $CO_2$. To avoid cross-contamination by potentially incomplete combustion, each sample was followed by a blank. Free blanks (placed away from samples) of carbon and nitrogen were monitored with empty tin capsules, and their average peak area (0.03–0.04 Vs for $N_2$ and 1.6–2.2 Vs for $CO_2$) was

**Table 1**
List of samples, rock types and geographic positions. Ol = olivine, amph = amphibole.

| Sample | Latitude | Longitude | Description |
|---|---|---|---|
| 562,544 | 66.41457 | −38.1364 | Ultramafic rock (ol + amph) |
| 562,553 | 66.41924 | −38.1707 | Rusty silica-rich schist |
| 562,555 | 66.46294 | −38.3732 | Rusty silica-rich schist |
| 562,557 | 66.46211 | −38.3745 | Rusty silica-rich schist |
| 562,565-A | 66.3602 | −37.7193 | Marble |
| 562,565-B | 66.3602 | −37.7193 | Marble |
| 562,572 | 66.36642 | −37.7095 | Marble |
| 562,576 | 66.38614 | −37.6896 | Sulfide-rich schist |
| 562,577 | 66.38595 | −37.6900 | Sulfide-rich schist |
| 564,936 | 66.35602 | −37.0888 | Marble |
| 564,937 | 66.35602 | −37.0888 | Marble |
| 564,940 | 66.35602 | −37.0888 | Marble |
| 564,945 | 66.36237 | −37.0972 | Graphitic schist |
| 564,946 | 66.36239 | −37.0973 | Graphitic gneiss |
| 564,988 | 66.24491 | −38.0186 | Sulfide-rich schist |
| 564,989 | 66.24487 | −38.0184 | Sulfide-rich schist |

subtracted from all samples and standards within the same run. Measurements where the sample/blank ratio of total peak areas (i.e. integrated over all isotopologues) was smaller than 5 were discarded. For nitrogen, the sample peaks were too small to measure nitrogen isotope ratios (all <0.5 Vs). However, carbon isotopes could be measured for all samples with sample/blank ratios mostly well above 10. The carbon isotope data were converted to the standard delta notation relative to Vienna Peedee Belemnite ($\delta^{13}C = [(^{13}C/^{12}C)_{sample}/(^{13}C/^{12}C)_{VPDP} - 1] \cdot 1000$) by calibration to the international reference materials USGS-40 and USGS-41. For the standards, also nitrogen isotope ratios were measured, relative to average air ($\delta^{15}N = [(^{15}N/^{14}N)_{sample}/(^{15}N/^{14}N)_{air} - 1] \cdot 1000$). The standard USGS-62 was used as a quality control for the isotopic calibration, and the results ($\delta^{13}C = -14.73 \pm 0.12$ ‰; $\delta^{15}N = +20.26 \pm 0.36$ ‰; 2σ) were in good agreement with expected values ($\delta^{13}C = -14.79 \pm 0.04$ ‰, $\delta^{15}N = +20.17 \pm 0.06$ ‰). Replicate measurements of the industrial graphite powder USGS-24 gave a value of $-16.07 \pm 0.26$ ‰ (2σ), compared to an expected value of $-16.05 \pm 0.07$ ‰, which reveals good reproducibility and accuracy. In addition, we analysed two rock standards, SGR-1 and SDo-1, and our isotopic data (SGR-1: $\delta^{13}C = -29.52 \pm 0.80$ ‰, $\delta^{15}N = +17.95 \pm 0.79$ ‰; SDo-1: $\delta^{13}C = -30.16 \pm 0.58$ ‰, $\delta^{15}N = -0.44 \pm 0.48$ ‰; 2σ) turned out to be in good agreement with previous measurements (SGR-1: $\delta^{13}C = -29.3 \pm 0.1$ ‰, $\delta^{15}N = +17.4 \pm 0.4$ ‰; SDo-1: $\delta^{13}C = -30.0 \pm 0.1$ ‰, $\delta^{15}N = -0.8 \pm 0.3$ ‰; 2σ) (Dennen et al., 2006). Total organic carbon (TOC, where the term 'organic' is here loosely defined to include graphite) and total nitrogen (TN) abundances were calibrated with a series of USGS-41 with different masses. For TN, eight of the fifteen samples were analysed in replicates, and the average reproducibility was 24%, due to the very low TN abundances, which made these measurements challenging.

### 3.2. Major elemental abundances

For total major element concentrations, an aliquot of 0.5 g of untreated powder of each sample was sent to Australian Laboratory Services in Dublin, Ireland. The samples were analysed with method ME-MS61, which uses a four-acid digestion procedure ($HNO_3$, HCl, $HClO_4$, HF), followed by ICP-MS analyses. Analytical reproducibility was better than 3% (relative error) for all major elements. The two reference materials MRGeo08 and EMOG-17 were used for quality control, and the results were within 2% of the expected values. Sample 564,988 had a K-concentration below the detection limit of 0.01 wt%; this data point is therefore reported as 0.5 x the detection limit.

## 4. Results

All data from this study are shown in Tables 2 and 3. The carbon isotope values of the graphite ($\delta^{13}C_{graphite}$) range from −28.4 ‰ to −4.1 ‰ (Fig. 4), in general agreement with previous work on graphite from this area (Rosing-Schow et al., 2017). These authors show that such values can be generated through redox reactions between $CO_2$ and $CH_4$ at temperatures of roughly 600 °C. In our sample set, the highest $\delta^{13}C_{graphite}$ values tend to occur in samples with the highest carbonate content (*i.e*, in nearly pure marble) (Fig. 4), reflecting isotopic exchange between the two carbon phases. For the marble represented by sample 562,572, two measurements of the $\delta^{13}C_{carbonate}$ are available ($\delta^{13}C_{carbonate} = 0.62$ and 0.91 ‰, Crotty et al., 2022). Assuming isotopic equilibrium between the graphite and carbonate phases results in a temperature estimate of 635–670 °C for equilibration (using the calibration of Polyakov and Kharlashina, 1995).

The TOC concentration ranges from 0.004 wt% to 29.6 wt%, while TN concentrations are 0.2 and 16.3 μg/g. For the lowest TOC and TN abundances, modern contamination is possible, meaning that our measured concentration would be upper limits, which would strengthen our overall conclusions (see below). We also stress that the samples were washed with DI-water, methanol and HCl (Section 3) to remove contaminants. If contamination had been significant, we should not have been able to measure such low concentrations. Hence contamination is likely minor for most samples. The molar TOC to TN ratio (hereafter C/N for brevity) is inversely correlated with 1/TOC ($R^2 = 0.75$, $p < 0.0001$) (Fig. 5a), meaning that the purest graphite samples have the highest C/N ratios and vice versa. The linear trend can be extrapolated to 100% TOC (i.e., log(1/TOC) = −2), yielding a C/N ratio of 67,854. In reality, graphite may not exist in its purest form with 100% C, because it might contain impurities such as N, as well as H and O. Therefore, the C/N ratio of the graphite alone (i.e., without the silicate phase) likely falls between 28,044 (the highest measured ratio) and 67,854.

Nevertheless, TN is positively correlated with TOC ($R^2 = 0.58$, $p < 0.001$, Fig. 5c), which might indicate that the graphite remains a significant host phase of nitrogen in these rocks. This inference is also supported by a mixing model (Fig. 5b), which produces the best fit with the data for 1 μg/g silicate-bound N and $\log(C/N)_{graphite}$ of 4.5. Alternatively, the covariance could reflect a common source for C and N without necessarily being contained in the same host phase. The samples with low TOC, which are closest to the pure silicate endmember, contain less than a few μg/g of nitrogen. TN is weakly correlated with total K

**Table 2**
Major elemental abundances, excluding Si, which was not determined. Note that sample 562,565-A was not analysed. * = the concentration is reported as 0.5 x the detection limit of 0.01 wt%.

| Sample | Al [wt %] | Ca [wt %] | Fe [wt %] | K [wt %] | Mg [wt%] | Na [wt %] | S [wt %] |
|---|---|---|---|---|---|---|---|
| 562,544 | 6.18 | 1.35 | 0.95 | 1.60 | 1.69 | 2.47 | 0.14 |
| 562,553 | 6.07 | 1.17 | 0.03 | 2.98 | 0.01 | 2.8 | 0.21 |
| 562,555 | 7.51 | 2.97 | 4.37 | 1.36 | 1.49 | 1.78 | 1.45 |
| 562,557 | 9.06 | 3.15 | 4.46 | 3.68 | 1.44 | 1.98 | 1.57 |
| 562,565-B | 5.95 | 10.15 | 1.80 | 0.66 | 9.97 | 1.69 | 0.005* |
| 562,572 | 0.10 | 21.4 | 0.17 | 0.07 | 12.70 | 0.01 | 0.01 |
| 562,576 | 7.93 | 6.83 | 1.94 | 0.22 | 1.24 | 1.75 | 0.41 |
| 562,577 | 7.13 | 9.06 | 4.32 | 0.23 | 1.75 | 0.85 | 1.20 |
| 564,936 | 3.00 | 25.9 | 2.24 | 1.18 | 0.73 | 0.64 | 0.96 |
| 564,937 | 5.22 | 2.10 | 0.97 | 5.14 | 1.23 | 0.88 | 0.03 |
| 564,940 | 6.21 | 2.43 | 2.08 | 0.46 | 0.36 | 2.90 | 1.06 |
| 564,945 | 3.48 | 7.94 | 9.6 | 2.16 | 3.13 | 0.48 | 0.03 |
| 564,946 | 0.62 | 1.71 | 0.98 | 0.50 | 0.90 | 0.12 | 0.74 |
| 564,988 | 0.07 | 20.1 | 4.06 | 0.005* | 10.55 | 0.02 | 2.22 |
| 564,989 | 5.00 | 9.23 | 13.15 | 0.08 | 2.29 | 0.05 | 4.93 |

**Table 3**
Graphite carbon and nitrogen data for decarbonated residues and total carbonate content. C/N is shorthand for TOC/TN.

| Sample | TOC [wt %] | $\delta^{13}C_{graphite}$ [‰] | TN [μg/g] | C/N [mol/mol] | Carbonate [wt%] |
|---|---|---|---|---|---|
| 562,544 | 0.044 | −28.38 | 0.45 | 1140 | 8.5 |
| 562,553 | 0.843 | −28.38 | 2.08 | 4722 | 4.6 |
| 562,555 | 0.032 | −19.16 | 1.47 | 255 | 14.4 |
| 562,557 | 0.151 | −18.86 | 1.27 | 1386 | 11.9 |
| 562,565-A | 0.006 | −16.97 | 0.60 | 113 | 13.4 |
| 562,565-B | 0.004 | −17.42 | 1.18 | 36 | 10.2 |
| 562,572 | 0.312 | −4.07 | 0.47 | 7715 | 98.2 |
| 562,576 | 0.120 | −14.51 | 0.54 | 2583 | 12.0 |
| 562,577 | 0.264 | −14.64 | 2.27 | 1354 | 20.5 |
| 564,936 | 0.610 | −9.81 | 11.12 | 640 | 67.6 |
| 564,937 | 29.562 | −18.68 | 16.33 | 21,113 | 4.2 |
| 564,940 | 0.411 | −13.61 | 2.75 | 1745 | 7.4 |
| 564,945 | 8.398 | −26.39 | 3.49 | 28,044 | 11.6 |
| 564,946 | 1.859 | −22.75 | 4.48 | 4839 | 2.6 |
| 564,988 | 0.005 | −13.02 | 0.20 | 312 | 59.3 |
| 564,989 | 0.021 | −11.04 | ND | ND | 13.6 |

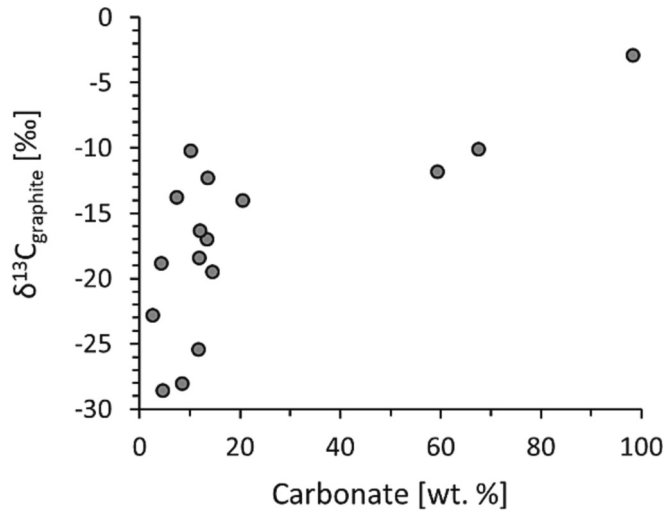


**Fig. 4.** Graphite carbon isotopes versus carbonate content. Although this graphite is hydrothermal and abiotic in origin, the isotopic values are comparable to metamorphosed biogenic carbon, meaning that they cannot be used as a biosignature and other proxies such as nitrogen chemistry are needed.

concentrations ($R^2 = 0.33$, $p = 0.03$) (Fig. 5d).

## 5. Discussion

### 5.1. Comparison to Paleoarchean metasedimentary graphite

Our results indicate that pure hydrothermal graphite from this site would have a molar C/N ratio >28,000 and likely closer to 67,854 (especially if some of the N is silicate-hosted), which raises the question if such high C/N ratios can be a diagnostic feature of abiotic graphite. Biogenic graphite forms from biomass with a ratio of around 7–10 (Godfrey and Glass, 2011), but this ratio increases during metamorphism, as functional groups, relatively enriched in N, are progressively removed from the buried organic matter (Hayes et al., 1983). Hence, samples with biogenic graphite of amphibolite-facies metamorphic grade can display C/N ratios of several hundred to a few thousand (Fig. 6). For example, samples from the Mesoarchean Duffer Formation in Western Australia (3.47 Ga) have C/N ratios in extracted kerogen of 14,000–19,000 (Stüeken et al., 2017). The Duffer Formation is a 200 m-thick metamorphosed black shale within a demonstrably sedimentary succession (Wille et al., 2013), and so the biogenicity of this organic material cannot easily be questioned. However, are these ratios systematically lower than those of abiotic graphite with a similar thermal history?

For organic extracts from metasedimentary rocks in Isua (3.7 Ga), Strauss and Moore (1992) documented C/N ratios of 1000 (Fig. 6), which could suggest biogenicity because the values are much lower than in the Paleoproterozoic hydrothermal graphite analysed in this study. However, more recently, van Zuilen et al. (2005) reported 9.7 μg/g nitrogen for a graphite extract from the Rosing locality at Isua (combining

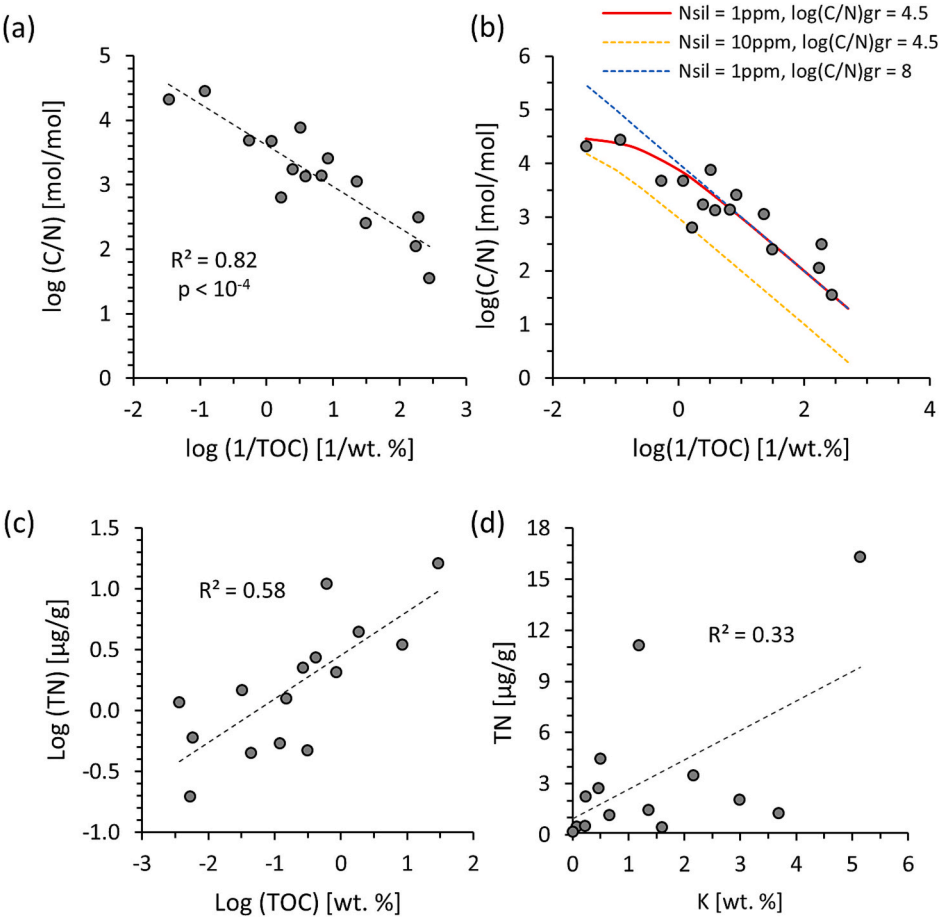


**Fig. 5.** Elemental abundances in hydrothermal graphite from this study. (a) The molar ratio of TOC to TN (abbreviated C/N) versus 1/TOC, showing that the purest graphite (lowest 1/TOC) has the highest C/N ratio of over 24,000. (b) Mixing models with different amounts of silicate-bound N and C/N ratios in graphite. The best fit with the data is achieved with 1 ppm $N_{silicate}$ and $\log(C/N)_{graphite}$ of 4.5. (c) TN versus TOC. The positive correlations shows that the nitrogen present in these rocks tends to be associated with graphite. The graphite-poor endmember (lowest TOC) has TN concentrations of a few ppm or less. (d) TN versus K, which are only weakly correlated with each other.

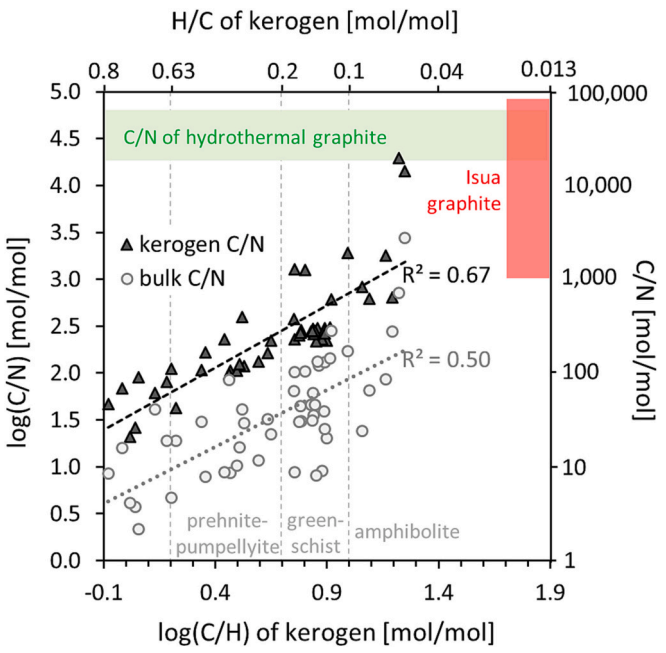


**Fig. 6.** Effects of metamorphism on C/N and C/H ratios of organic matter, modified from Stüeken et al. (2017). The C/N ratio for hydrothermal graphite (green band) is from this study and ranges from the measured lower limit to the calculated upper limit. The range indicated for Isua (red box) spans the two data points taken from the literature (Strauss and Moore, 1992; van Zuilen et al., 2005). All other data points included in the figure are from various metasedimentary rocks as described by Stüeken et al. (2017) to illustrate the trend. (For interpretation of the references to colour in this figure legend, the reader is referred to the web version of this article.)

their data points from combustion steps at 550–800 °C), which would equate to a C/N ratio of 82,474 if the carbon content of the graphite extract is assumed to be on the order of 80% (not reported in their study). For a less pure graphite extract with 50% carbon content (the residuum being made up of HF-insoluble minerals like pyrite, zircon etc.), the C/N ratio would be 51,546. These values are much higher than in the Duffer Formation and more similar to the Paleoproterozoic hydrothermal graphite deposit, which may indicate an abiotic origin of Isua graphite. Indeed, van Zuilen et al. (2005) proposed that the nitrogen in their graphite samples from Isua was of abiotic origin, based on the isotopic similarity between epigenetic graphite in siderite veins and putatively syngenetic graphite from mica schists. However, the data from the Duffer Formation in Australia appear to fall off the metamorphic trend for biogenic graphite when plotted against C/H ratios (Fig. 6). In contrast, the Isua data, which have higher C/H ratios (Strauss and Moore, 1992), may follow the trend and thus conform with a biogenic origin. Therefore C/N ratios alone cannot unambiguously distinguish hydrothermal from biogenic graphite. Other indicators are needed to assess biogenicity.

Looking at the bulk rock data from this study (Fig. 5), the overall trends found in the samples of the hydrothermal graphite deposit contrasts with those from graphitic metapelites from Isua, where TN is uncorrelated with TOC (Fig. 7b) and instead strongly correlated with K (Fig. 7c) (Stüeken et al., 2021). Those graphitic metapelites are the same geological unit as that originally studied by Rosing (1999). We focus on those rocks in this discussion, because bulk rock data are available (Stüeken et al., 2021), and they have a moderately high carbon content, compared to Paleoarchean rocks where graphite has been documented only in mineral inclusions (e.g., Mojzsis et al., 1996). In these graphitic metapelites from Isua, samples with >2 wt% K contain >20 μg/g of nitrogen, suggesting that a significant fraction of the total nitrogen content is hosted in potassic silicate minerals (Stüeken et al., 2021). This phenomenon is well known from other metasedimentary successions in the rock record where TN and K are strongly correlated (reviewed by Busigny and Bebout, 2013), and it is consistent with independent measurements of nitrogen in biotite separates, which contain several tens to hundreds of μg/g (Fig. 7a) (Honma, 1996; Pinti et al., 2001; Papineau et al., 2005). During diagenetic alteration of biomass within sediments, ammonium is released into pore waters, where it can reach concentrations of several millimole per litre (Rosenfeld, 1979; Boudreau and Canfield, 1988). The dissolved ammonium then substitutes into potassic clay minerals (Müller, 1977; Schroeder and McLain, 1998), which later transform into micas and feldspars during metamorphism. K-silicates are therefore a significant reservoir of nitrogen in Earth's crust. In the case of the hydrothermal graphite deposit, however, nitrogen appears to be depleted relative to potassium in most samples (Fig. 8), although K concentrations extend over a similar range as in the Isua metapelites. This observation suggests that ammonium concentrations were lower during the formation of the hydrothermal graphite deposit, such that potassic minerals did not become enriched in nitrogen to the same degree as they did in the Isua setting. This leads to the next question if the ammonium concentration of a graphite-forming fluid, which gets captured in potassic minerals, can be indicative of biogenicity.

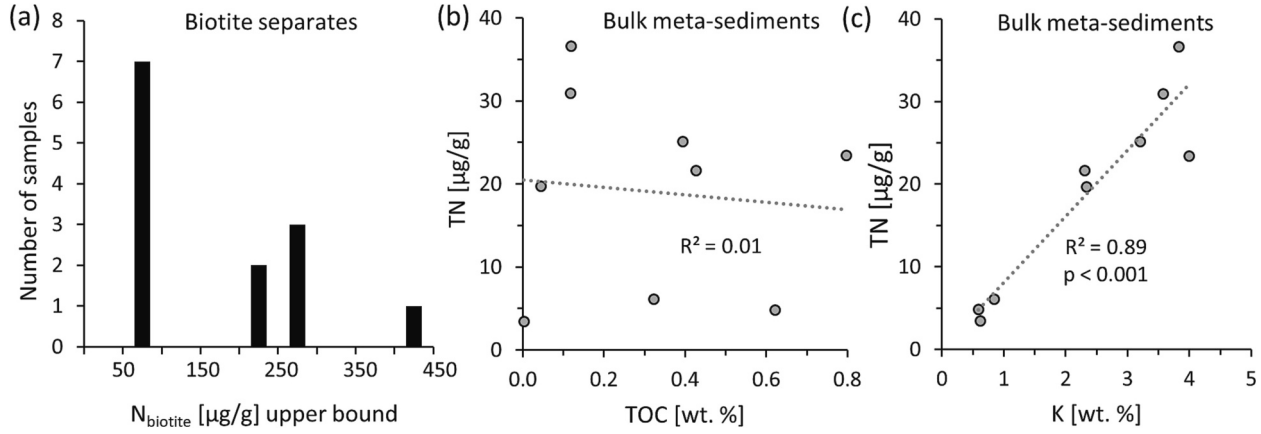


**Fig. 7.** (a) Nitrogen contents from biotite separates from Isua metapelits, taken from Stüeken et al. (2016) and references therein. (b) TN versus TOC for graphitic metapelites from Isua, from the same geological unit as studied by Rosing (1999), and (c) TN versus K for the same samples as in panel (b), data taken from Stüeken et al. (2021). The graphitic metapelites from Isua are used here for comparison because bulk rock data are available and carbon contents are higher than in other Paleoarchean settings where graphite has primarily been detected in mineral inclusions.

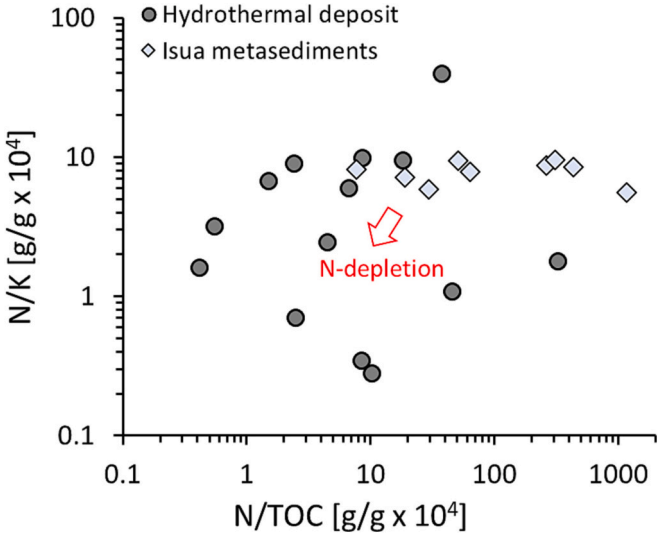


**Fig. 8.** Comparison of N/K and N/TOC ratios of the hydrothermal graphite deposit from this study and metasedimentary data from the graphitic metapelites from Isua, taken from Stüeken et al. (2021). As noted above, we focus on those metapelites for comparison, because whole-rock data are available, and they contain moderate amounts of carbon that has previously been linked to early life (Rosing, 1999; Hassenkam et al., 2017). The data reveal N-depletion relative to TOC and in particular relative to K in the hydrothermal graphite deposit of this study, compared to the Isua metapelites from the Rosing (1999) locality.

### 5.2. *Thermodynamic modelling of abiotic nitrogen in association with graphite*

Abiotic ammonium enrichment in clay minerals was previously explored with an empirically-calibrated hypothetical abiotic nitrogen cycle for the global ocean (Stüeken, 2016), and results indicated that only up to a few μg/g of N in phyllosilicate minerals could be of abiotic origin. In this study, the presence of graphite is used to develop an independent thermodynamic approach for the formation of abiotic N-enrichments. First, graphite formation was modelled with the GEM Selector software package, version 3.7 (Kulik et al., 2013). The elemental composition was set to C, H, O, and N. Several models were run, where the abundances of C and N were held constant while the proportions of O and H were varied, such that C and N speciation could be monitored along horizontal trajectories in a CHO-ternary diagram (Fig. 9, coloured dots). We focused on the area around the graphite phase boundary within the ternary diagram, because the graphite in our samples co-exists with micas (Fig. 3), indicating that $H_2O$ was present during graphite formation. We have not incorporated other elements or mineral phases into the model, because we specifically want to explore how the thermodynamic stability of graphite impacts the redox speciation of N in the system. Nitrogen incorporation into silicate minerals depends primarily on whether N occurs in the form of ammonium (N(-III)) or $N_2$ (N(0)), and our model approach allows us to test which redox state of N is favoured within the regime that allows carbon to exist in the form of graphite. The emphasis on horizontal transects in the model may replicate the conditions under which graphite forms, i.e. from a fluid with a fixed carbon content that contains oxidized ($CO_2$) and reduced ($CH_4$) endmembers that reorganize into graphite. For nitrogen, two C:N ratios of 10 and 1 were tested to explore the effects of this ratio on nitrogen speciation This choice is further discussed below. The models were run at either 400 °C or 600 °C. The graphite samples analysed in this study formed after terrane juxta-positioning and peak metamorphism, with an initial metasomatic event at around 600 °C (Rosing-Schow et al., 2017), and a later (remobilisation) at greenschist facies conditions of around 400 °C (Section 2.2). The pressure in the model was set to 5 kbar for the 600 °C run, which is a plausible pressure, considering that the rocks started at peak metamorphic conditions of 750 °C and 8 kbar, and this metasomatic event occurred later. For the 400 °C model, a pressure of 2 kbar was used. These two sets of pressure-temperature conditions correspond approximately to upper greenschist and mid-amphibolite facies. In particular the high-temperature model is also a suitable approximation for the Isua samples (Ramírez-Salazar et al., 2021).

As expected, the results show that the N(-III)/N(0) ratio is highest near the H-apex of the ternary diagram. We therefore ran models at higher resolution at a carbon fraction of 15% to explore how N speciation evolves across the graphite phase boundary (Fig. 10). This analysis shows that the abundance of graphite (stability indicated by grey shading in Fig. 10) relative to total carbon increases up to a H:O ratio of

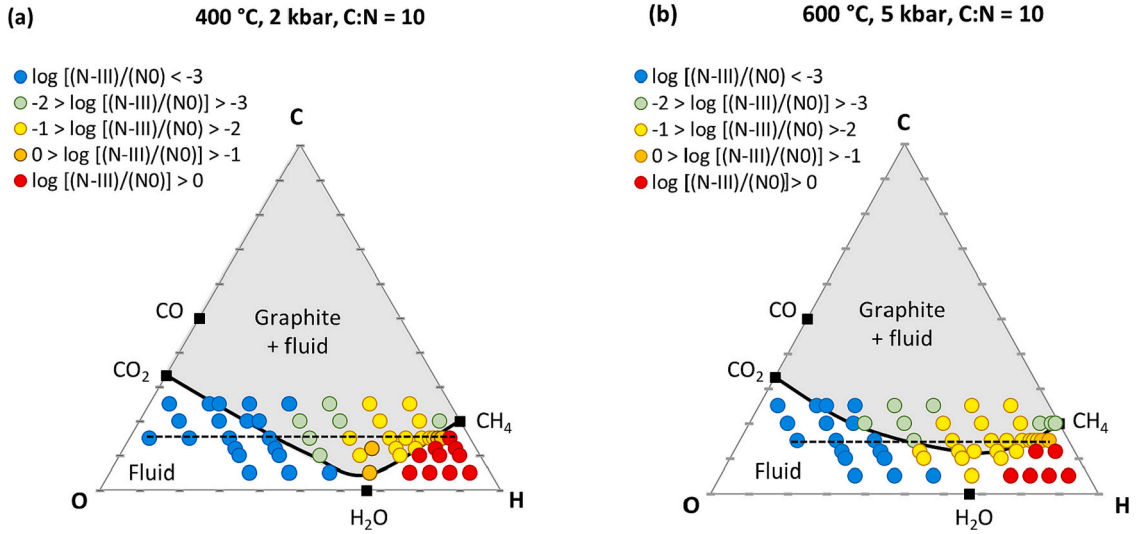


**Fig. 9.** Ternary diagrams of graphite stability (grey shaded area) in carbon-oxygen-hydrogen space for 400 °C and 2 kbar (a) and 600 °C and 5 kbar (b). The modelled graphite stability fields are consistent with the literature (Huizenga, 2011). Plotted on top of the graphite stability fields are ratios of N(-III)/N(0) (coloured circles), at a C:N ratio of 10. Models with C:N ratios of 1 were also run but are not shown. The black dashed line represents a set of models where nitrogen speciation was investigated in greater detail, because the N(-III)/N(0) ratio was highest near the graphite stability edge (see Fig. 10). In our sample set, graphite co-exists with micas (Fig. 3), indicating that the fluid that formed the graphite contained water and was thus situated somewhere along the phase boundary of graphite.

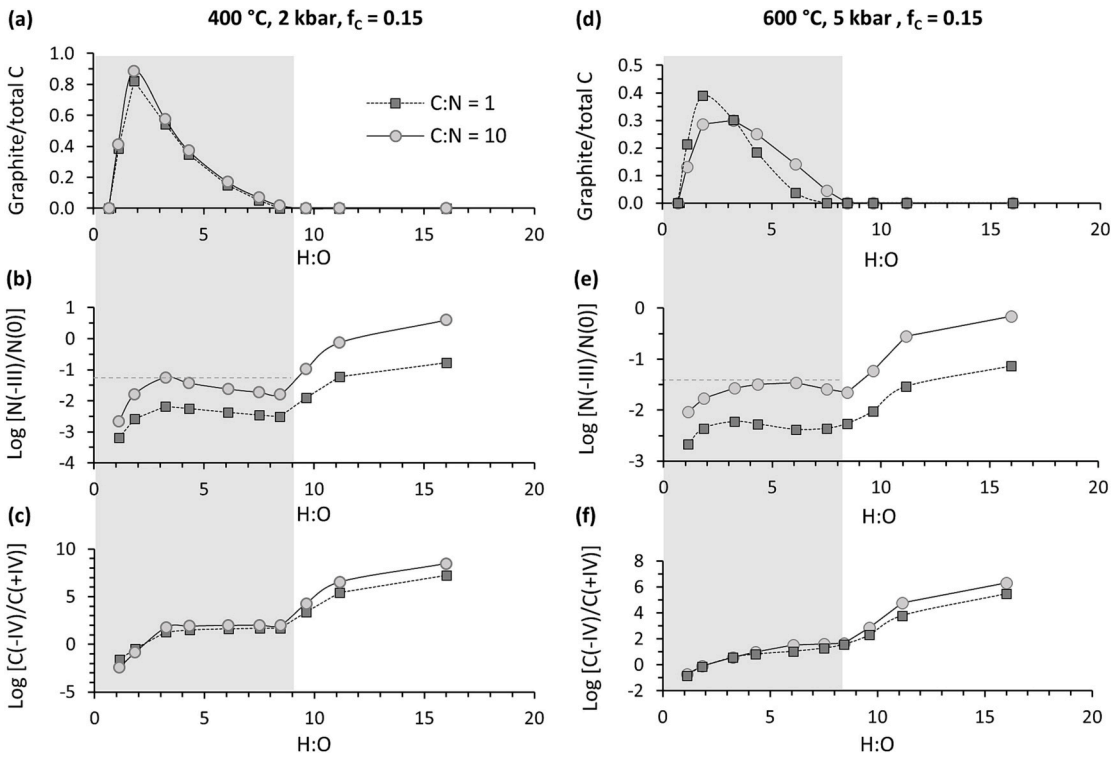


**Fig. 10.** Model results for 400 °C at 2 kbar (a-c) and 600 °C at 5 kbar (d-f) along the horizontal trajectories indicated by black dashed lines in Fig. 9. Grey shading = graphite is present. As graphite abundance increases with decreasing H:O, the C(-IV)/C(+IV) ratio is relatively constant (c, g). Also the N(-III)/N(0) ratio is buffered in this range (d, h), likely because increasing graphite abundance prevents further reduction of C and N. After peak graphite abundance has been reached, both N (-III)/N(0) and C(-IV)/C(+IV) drop. Since graphite coexists with hydrated silicates in our settings (both in the hydrothermal graphite deposit and in the Isua metapelites), the most relevant points are on the graphite phase boundary, at H:O ratios of around 9 in (a)-(c) and H:O ratios around 8.5 in (d)-(f).

about 2 but decreases again at lower H:O ratios. While the abundance of graphite increases, the C(-IV)/C(+IV) ratio (Fig. 10c,f) is buffered to a constant value, whereas at more reducing conditions, the system is strongly dominated by C(-IV) (i.e., methane, $CH_4$), and once peak graphite abundance has been reached, C(+IV) (i.e., $CO_2$) becomes relatively more abundant.

Similar to carbon, also nitrogen speciation is strongly dominated by the most reduced form N(-III) (i.e., $NH_4^+$) relative to N(0), (i.e., $N_2$) when the H:O ratio is high (Fig. 10b,e), and the N(-III)/N(0) ratio is buffered to a constant ratio while the graphite reservoir is growing. With decreasing H:O, the N(-III)/N(0) ratio decreases further. Hence the results show that the speciation of nitrogen is strongly impacted by the presence of graphite, which buffers the redox state of the system. Therefore, the presence of graphite in the rock record can provide thermodynamic constraints on the relative abundance of ammonium in a fluid. This raises the next question of whether this relative constraint can be translated into an absolute N abundance in the rock that can be used as a reference point to assess biogenicity. To do that, we need (a) an estimate of the maximum plausible abiotic N concentration in aqueous fluids relative to carbon, and (b) the degree of ammonium partitioning into potassic minerals that are in equilibrium with this fluid.

The largest reservoir of nitrogen at the Earth's surface is in the atmosphere, and therefore the most effective way to generate an abiotic fluid enriched in dissolved N is by dissolving $N_2$ in seawater. The solubility of $N_2$ in seawater at 4 °C is 0.8356 mmol/L, which was determined with a simple equilibrium model in Geochemist's Workbench®, where seawater salt solution with modern abundances was put in equilibrium with an $N_2$ gas fugacity of 0.8. The total gas pressure was kept at 1 bar, because ocean water acquires its dissolved gas inventory at the seawater-atmosphere interface and carries this inventory into the deep ocean and crust from there (e.g., Nicholson et al., 2010). Hence the effects of pressure on $N_2$ solubility do not affect the total dissolved inventory any further. We can therefore use this fluid as a plausible abiotic N source to calculate the maximum abiotic ammonium concentration that could be generated in the stability field of graphite, given the thermodynamic constraints calculated above. We note that there are hydrothermal fluids with over 10 mmol/L of ammonium, but there the ammonium is remobilized from organic-rich sediments (von Damm, 1990; Lilley et al., 1993) and is therefore not truly abiotic in origin. Hydrothermal vents that are not associated with any sediment cover have much lower ammonium levels of less than the detection limit of 0.01 mmol/L (Lilley et al., 1993). Using the total dissolved $N_2$ reservoir of 0.8356 mmol/L as a potential source of ammonium under appropriate redox conditions is therefore a conservative upper limit.

In seawater, the concentration of dissolved inorganic carbon is around 2.0–2.3 mmol/L (e.g., Dore et al., 2009), meaning that the abiotic C:N ratio of the total dissolved gases is 2.4–2.8, i.e. between our modelled ratios of 1 and 10 shown in Fig. 10. Many hydrothermal fluids have total carbon concentrations within a factor of 2–5 times that of seawater (von Damm, 1990), meaning that the C:N ratio (where most N is $N_2$ rather than biomass-recycled ammonium, see above) still falls close to our modelled ratio of 10. We will continue to use both C:N ratios of 1 and 10 as plausible bounds. As indicated in Fig. 10b,e, the N(-III)/N(0) ratio near the phase boundary of graphite at the assumed PT conditions is at most $10^{-1}$. In a separate set of models we further explored the effects of P and T, but this upper limit of $10^{-1}$ for the N(-III)/N(0) ratio held up (see Appendix). More specifically, most hydrothermal graphite forms at temperatures >500 °C (Luque et al., 2009), and the N(-III)/N(0) ratio was found to decrease with temperature (compare Appendix Fig. S2 and S3). Pressure has a relatively lessor effect. Hence a value of $10^{-1}$ is an upper limit, and the true maximum value is likely closer to $10^{-2}$ (Fig. 10). In other words, at most 10% and more likely <1% of the dissolved $N_2$ is converted to ammonium under the redox conditions where graphite precipitates.

Next, we converted this dissolved ammonium concentration into a hypothetical mineral concentration that could be obtained abiotically under high-temperature conditions. The conversion was based on partition coefficients derived by Pöter et al. (2004) and Moin et al. (1994) for muscovite, biotite and K-feldspar in equilibrium with a saline fluid at 400–600 °C and 4–15 kbar. These partition coefficients, defined as the ratio of ammonium in the fluid to ammonium in the mineral, range from 4 to 8 for muscovite and feldspar and are as low as 2 for biotite. They are applicable under conditions where $NH_4^+$ concentrations are significantly lower than $K^+$ concentrations, i.e. where N levels are so low that they do not impact the thermodynamic stability of K-minerals, which is valid for systems with up to a few hundred μg/g of silicate-bound N and therefore valid for both the hydrothermal graphite deposit and for the Isua metapelites. The pressure-temperature dependence of this partition coefficient is minor (Pöter et al., 2004). Using 2 and 8 as lower and upper bounds, we then calculated the concentration of mineral-bound ammonium for different water/rock ratios (Fig. 11a). The water/rock ratio describes how much fluid is in equilibrium with a given amount of rock. A realistic water/rock ratio for average shales is 1.3 by mass (Robb, 2005), as muds are known to lose roughly 3500 L of water per final 1 $m^3$ of dehydrated sedimentary rock. This ratio would be valid for the Isua samples, which are interpreted as turbidites (Rosing, 1999). In the Isua samples, the K-concentrations of 0.6–4% (Fig. 7c) indicate that only a fraction of the rock is made of potassic minerals. Pure orthoclase contains 14.0% K while pure muscovite contains 9.8% K. Scaling the realistic total water/rock ratio of 1.3 by the fraction of potassic minerals therefore lowers the effective water/rock ratio that is relevant for calculating bulk rock nitrogen enrichments. In other words, the rock can only take up a fraction of the total ammonium from the fluid, if fewer appropriate mineral phases are available that can accommodate $NH_4^+$ in their structure, and hence only a smaller proportion of the fluid is sampled by a given amount of rock. Overall, the results (Fig. 11b) show that <1 μg/g of nitrogen can be derived by this abiotic mechanism in the Isua samples. The plausible upper limit with this calculation is 0.3 μg/g for a rock with 41% of potassic mineral phases that are capable of assimilating ammonium.

For the hydrothermal graphite deposit, the water/rock ratio may be higher than in marine mud but is difficult to constrain. Wetzel and Shock (2000) estimated a water/rock ratio of <5 in high-temperature submarine hydrothermal systems. Similar ratios were also used successfully in simulations of such systems by Alt-Epping and Smith (2001) and in experiments by Ueda et al. (2016). Our hydrothermal graphite formed in an intracontinental setting, where water is likely less abundant. Therefore, a water/rock ratio of 5 may be a useful upper limit. The effective ratio would be 2–28 times lower for whole-rocks with 0.5–51% K. Using this constraint, our data for the hydrothermal graphite deposit (Fig. 5) show that this abiotic mechanism could potentially explain the low N-content of around 1 μg/g in the most graphite-poor samples, i.e. in those samples where the graphite contribution to the TN content is minimal. In the case of the Isua samples (Fig. 7), none of the samples are explicable by this abiotic mechanism alone; a large proportion of additional N must have been derived from other sources. The most N-poor samples may include detrital components from magmatic minerals that can contain a few μg/g of nitrogen (Johnson and Goldblatt, 2015; Stüeken et al., 2021); however, the majority of the data points with >10 μg/g are most parsimoniously explained by a much more ammonium-rich fluid that equilibrated with the potassic minerals prior to graphitization, and the most plausible source for such an ammonium-rich fluid is the degradation of organic matter within sedimentary pore waters. The N-content of the silicate endmember is therefore preserving indirect evidence of a past biosphere in these metasediments at Isua.

## 6. Conclusions

Many of the oldest putative traces of life on Earth are in the form of graphite; however, proving the biogenicity of these graphite occurrences has been challenging. While biogenic organic matter can transform into graphite during metamorphism, graphite can also form abiotically from reactions with $CO_2$, CO and/or $CH_4$ gases, given appropriate redox and pressure-temperature conditions. Some previous workers used the isotopic composition of nitrogen contained in Paleoarchean graphite to argue against a biogenic origin (van Zuilen et al., 2005), but others have used the presence of carbon-bound nitrogen, along with oxygen and minor phosphorus as an indicator for past life (Hassenkam et al., 2017). Our data from a *bona fide* hydrothermal graphite deposit of Paleoproterozoic age suggest that abiotic graphite may contain nitrogen with C/N ratios that are comparable to remnants of ancient biomass in the Archean rock record, including rocks from Isua (3.7 Ga) and from the

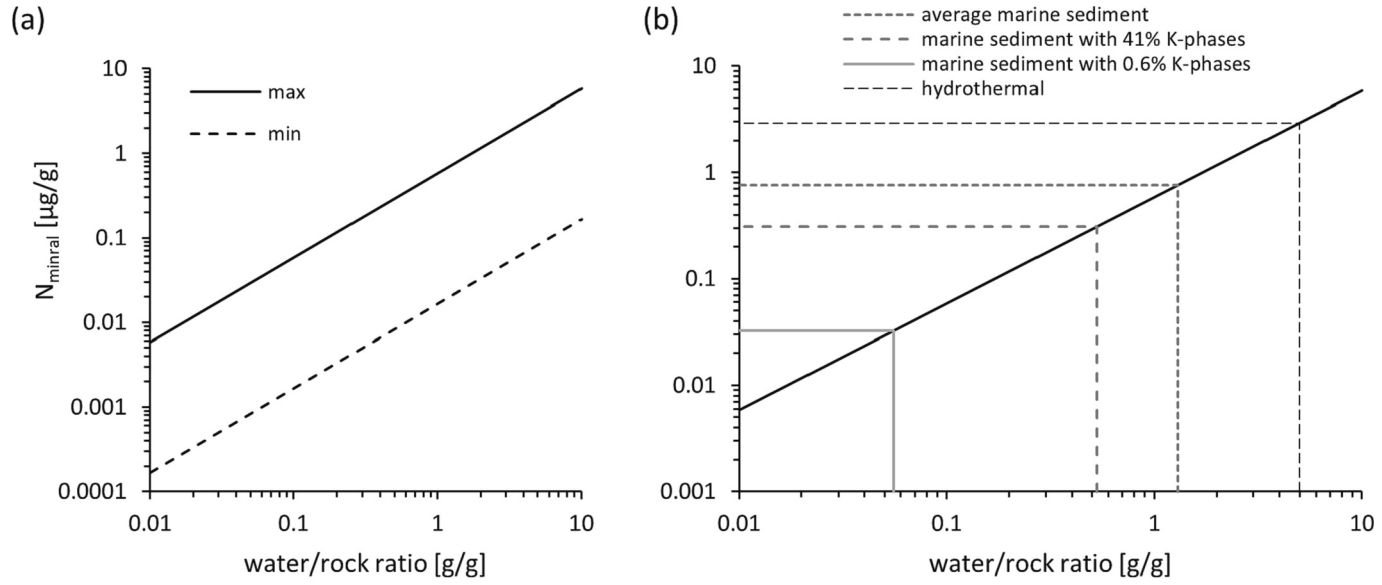


**Fig. 11.** Calculation of plausible abiotic NH4+ contents in potassic minerals. (a) Maximum and minimum estimates as a function of water/rock ratio, based on plausible upper and lower bounds for input parameters (see text). (b) Zoom into the maximum curve from (a) and highlighting realistic water/rock ratios in marine sediments relevant for the Isua metapelites as well as a plausible water/rock ratio for high-temperature hydrothermal settings (Wetzel and Shock, 2000). Also highlighted are scaled water/rock ratios for the K-abundances reported for the Isua samples (Fig. 7c).

Pilbara craton (3.5 Ga). We stress that our inference of graphite-hosted N in the hydrothermal veins is at present only based on a the correlation between TOC and TN and a corresponding mixing model and has not been verified by N-speciation studies, which would be difficult to perform on rock with such low overall TN contents; however, previous studies have shown that graphite as such is capable of up-taking N-impurities (van Zuilen et al., 2005; Hassenkam et al., 2017), and therefore it is conceivable that also this hydrothermal graphite hosts some of the measured N. The nitrogen content of graphite alone can thus not be used as a strong indicator of biogenicity. However, we also find that the associated silicate rock that hosts the hydrothermal graphite investigated in this study is unusually N-depleted with endmember concentrations of around 1 μg/g or less. New thermodynamic models reveal that such low concentrations in both hydrothermal deposits and in metasediments are consistent with a non-biological ammonium source. In contrast, higher concentrations of several tens of μg/g, such as those found in graphite-bearing metapelites in the Isua supracrustal belt (Stüeken et al., 2021), are not explicable by a plausible abiotic source, because (a) the presence of graphite buffers the redox speciation of dissolved nitrogen with preference towards $N_2$ over $NH_4^+$ and (b) plausible abiotic fluid sources are unlikely to contain high levels of dissolved N. These high TN concentrations found in K-silicates require very high dissolved ammonium levels that are most parsimoniously explained by the breakdown of biomass within sediments prior to graphitization. We therefore conclude that potassic silicates, which have the potential to assimilate ammonium into their crystal lattice, can serve as an indirect way of evaluating the biogenicity of associated graphite. Applying this proxy to the Isua metapelites suggests that life on Earth dates back to at least 3.7 Ga.

## Declaration of Competing Interest

The authors declare that they have no known competing financial interests or personal relationships that could have appeared to influence the work reported in this paper.

The authors declare the following financial interests/personal relationships which may be considered as potential competing interests:

Eva Stueeken reports financial support was provided by Natural Environment Research Council.

## Data availability

All new data presented in this study are included in Tables 1-3 in the main text.

## Acknowledgements

This study was financially supported by a NERC Frontiers grant (NE/V010824/1) to EES and an Osisko research stipend to VvH. The samples were collected during fieldwork in 2014 in south-east Greenland as part of the SEGMENT project organised and led by GEUS, and co-financed by GEUS and MMR. We thank two anonymous reviewers for constructive comments that improved the manuscript.

## Appendix A. Supplementary data

Supplementary data to this article can be found online at https://doi.org/10.1016/j.chemgeo.2022.121274.

## References

Abramov, O., Mojzsis, S.J., 2009. Microbial habitability of the Hadean Earth during the late heavy bombardment. Nature 459, 419–422.
Alt-Epping, P., Smith, L., 2001. Computing geochemical mass transfer and water/rock ratios in submarine hydrothermal systems: implications for estimating the vigour of convection. Geofluids 1, 163–181.
Bell, E.A., Boehnke, P., Harrison, T.M., Mao, W.L., 2015. Potentially biogenic carbon preserved in a 4.1 billion-year-old zircon. Proc. Natl. Acad. Sci. 112, 14518–14521.
Boudreau, B.P., Canfield, D.E., 1988. A provisional diagenetic model for pH in anoxic porewaters: Application to the FOAM site. J. Mar. Res. 46, 429–455.
Boyd, S.R., 2001. Ammonium as a biomarker in Precambrian metasediments. Precambrian Res. 108, 159–173.
Busigny, V., Bebout, G.E., 2013. Nitrogen in the silicate Earth: Speciation and isotopic behavior during mineral–fluid interactions. Elements 9, 353–358.
Crotty, C., van Hinsberg, V., Szilas, K., Poulsen, M.D., 2022. Palaeoproterozoic arc related supracrustal units from the Tasiilaq Region, SE Greenland: Insights into the convergence of the Rae and North Atlantic Cratons. Precambrian Res. 379, p106808.
von Damm, K.L., 1990. Seafloor hydrothermal activity: Black smokers chemistry and chimneys. Annu. Rev. Earth Planet. Sci. 18, 173–204.
Dennen, K.O., Johnson, C.A., Otter, M.L., Silva, S.R., Wandless, G.A., 2006. $\delta^{15}N$ and non-carbonate $\delta^{13}C$ values for two petroleum source rock reference materials and a marine sediment reference material. U.S. Geol. Surv. Open-File Report 2006–1071.
Dore, J.E., Lukas, R., Sadler, D.W., Church, M.J., Karl, D.M., 2009. Physical and biogeochemical modulation of ocean acidification in the central North Pacific. Proc. Natl. Acad. Sci. 106, 12235–12240.
Fedo, C.M., Whitehouse, M.J., 2002. Metasomatic origin of quartz-pyroxene rock, Akilia, Greenland, and implications for Earth's earliest life. Science 296, 1448–1452.
Godfrey, L.V., Glass, J.B., 2011. The geochemical record of the ancient nitrogen cycle, nitrogen isotopes, and metal cofactors. Methods Enzymol. 486, 483–506.
Hall, R.P., Chadwick, B., Escher, J.C., Vasudev, V.N., 1989. Supracrustal rocks in the Ammassalik region, South-East Greenland. In: Kalsbeek, F. (Ed.), Geology of the Ammassalik Region, South-East Greenland. Grønlands Geologiske Undersøgelse (GGU), Copenhagen, pp. 17–22.
Hassenkam, T., Andersson, M.P., Dalby, K.N., Mackenzie, D.M.A., Rosing, M.T., 2017. Elements of Eoarchean life trapped in mineral inclusions. Nature 548, 78–81.
Hayes, J.M., Kaplan, I.R., Wedeking, K.W., 1983. Precambrian organic geochmistry, preservation of the record. In: Schopf, J.W. (Ed.), Earth's Earliest Biosphere - its Origin and Evolution. Princeton University Press, Princeton, NJ, pp. 93–134.
Honma, H., 1996. High ammonium contents in the 3800 Ma Isua supracrustal rocks, central West Greenland. Geochim. Cosmochim. Acta 60, 2173–2178.
Horita, J., 2001. Carbon isotope exchange in the system CO2-CH4 at elevated temperatures. Geochim. Cosmochim. Acta 65, 1907.
Huizenga, J.M., 2011. Thermodynamic modelling of a cooling C–O–H fluid–graphite system: implications for hydrothermal graphite precipitation. Mineral. Deposita 46, 23–33.
Itihara, Y., Suwa, K., 1985. Ammonium contents of biotites from Precambrian rocks in Finland: the significance of NH4+ as a possible chemical fossil. Geochim. Cosmochim. Acta 49, 145–151.
Johnson, B., Goldblatt, C., 2015. The Nitrogen budget of Earth. Earth Sci. Rev. 148, 150–173.
Kalsbeek, F., 1989. Geology of the Ammassalik Region, South-East Greenland. Geological Survey of Greenland, Copenhagen.
Kalsbeek, F., Austrheim, H., Bridgwater, D., Hansen, B.T., Pedersen, S., Taylor, P.N., 1993. Geochronology of Archaean and Proterozoic events in the Ammassalik area, South-East Greenland, and comparisons with the Lewisian of Scotland and the Nagssugtoqidian of West Greenland. Precambrian Res. 62, 239–270.
Kokfelt, T.F., Næraa, T., Thrane, K., Bagas, L., 2016. New zircon U-Pb and Hf isotopic constraints on the crustal evolution of the Skjoldungen region, South-East Greenland. GEUS Bull. 35, 55–58.
Kolb, J., 2014. Structure of the Palaeoproterozoic Nagssugtoqidian Orogen, South-East Greenland: model for the tectonic evolution. Precambrian Res. 255, 809–822.
Kueter, N., Schmidt, M.W., Lilley, M.D., Bernasconi, S.M., 2019. Experimental determination of equilibrium CH4–CO2–CO carbon isotope fractionation factors (300–1200 C). Earth Planet. Sci. Lett. 506, 64–75.
Kulik, D.A., Wagner, T., Dmytrieva, S.V., Kosakowski, G., Hingerl, F.F., Chudnenko, K.V., Berner, U.R., 2013. GEM-Selektor geochemical modeling package: revised algorithm and GEMS3K numerical kernel for coupled simulation codes. Comput. Geosci. 17, 1–24.
Lebrun, E., Árting, T.B., Kolb, J., Fiorentini, M., Kokfelt, T., Johannesen, A.B., Maas, R., Thébaud, N., Martin, L.A., Murphy, R.C., 2018. Genesis of the Paleoproterozoic Ammassalik Intrusive complex, south-East Greenland. Precambrian Res. 315, 19–44.
Lepland, A., van Zuilen, M.A., Arrhenius, G., Whitehouse, M.J., Fedo, C.M., 2005. Questioning the evidence for Earth's earliest life—Akilia revisited. Geology 33, 77–79.
Lilley, M.D., Butterfield, D.A., Olson, E.J., Lupton, J.E., Macko, S.A., McDuff, R.E., 1993. Anomalous CH4 and NH4+ concentrations at an unsedimented mid-ocean-ridge hydrothermal system. Nature 364, 45–47.
Luque, F.J., Ortega, L., Barrenechea, J.F., Millward, D., Beyssac, O., Huizenga, J.M., 2009. Deposition of highly crystalline graphite from moderate-temperature fluids. Geology 37, 275–278.
Moin, B., Guillot, C., Gibert, F., 1994. Controls of the composition of nitrogen-rich fluids originating from reaction with graphite and ammonium-bearing biotite. Geochim. Cosmochim. Acta 58, 5503–5523.
Mojzsis, S.J., Arrhenius, G., McKeegan, K.D., Harrison, T.M., Nutman, A.P., Friend, C.R., 1996. Evidence for life on Earth before 3,800 million years ago. Nature 384, 55–59.
Müller, P.J., 1977. CN ratios in Pacific deep-sea sediments: effect of inorganic ammonium and organic nitrogen compounds sorbed by clays. Geochim. Cosmochim. Acta 41, 765–776.
Müller, S., Dziggel, A., Sindern, S., Kokfelt, T.F., Gerdes, A., Kolb, J., 2018. Age and temperature-time evolution of retrogressed eclogite-facies rocks in the Paleoproterozoic Nagssugtoqidian Orogen, South-East Greenland: Constrained from

U-Pb dating of zircon, monazite, titanite and rutile. Precambrian Res. https://doi.org/10.1016/j.precamres.2018.1007.1002.
Nicholson, D., Emerson, S., Caillon, N., Jouzel, J., Hamme, R.C., 2010. Constraining ventilation during Deepwater formation using deep ocean measurements of the dissolved gas ratios 40Ar/36Ar, N2/Ar, and Kr/Ar. J. Geophys. Res. Oceans 115. https://doi.org/10.1029/2010JC006152.
Nicoli, G., Thomassot, E., Schannor, M., Vezinet, A., Jovovic, I., 2018. Constraining a Precambrian Wilson Cycle lifespan: an example from the ca. 1.8 Ga Nagssugtoqidian Orogen, Southeastern Greenland. Lithos 296, 1–16.
Nutman, A.P., Friend, C.R.L., 1989. Reconnaissance P, T studies of the Proterozoic crustal evolution of the Ammassalik area, South-East Greenland. In: Kalsbeek, F. (Ed.), Geology of the Ammassalik Region, South-East Greenland. Grønlands Geologiske Undersøgelse (GGU), Copenhagen, pp. 48–53.
Nutman, A.P., Kalsbeek, F., Friend, C.R., 2008. The Nagssugtoqidian orogen in South-East Greenland: evidence for Paleoproterozoic collision and plate assembly. Am. J. Sci. 308, 529–572.
Ohtomo, Y., Kakegawa, T., Ishida, A., Nagase, T., Rosing, M.T., 2014. Evidence for biogenic graphite in early Archaean Isua metasedimentary rocks. Nat. Geosci. 7, 25–28.
Papineau, D., Mojzsis, S.J., Karhu, J.A., Marty, B., 2005. Nitrogen isotopic composition of ammoniated phyllosilicates: case studies from Precambrian metamorphosed sedimentary rocks. Chem. Geol. 216, 37–58.
Papineau, D., De Gregorio, B.T., Cody, G.D., O'Neil, J., Steele, A., Stroud, R.M., Fogel, M. L., 2011. Young poorly crystalline graphite in the> 3.8-Gyr-old Nuvvuagittuq banded iron formation. Nat. Geosci. 4, 376–379.
Pinti, D.L., Hashizume, K., Matsuda, J.I., 2001. Nitrogen and argon signatures in 3.8 to 2.8 Ga metasediments: Clues on the chemical state of the Archean Ocean and the deep biosphere. Geochim. Cosmochim. Acta 65, 2301–2315.
Polyakov, V.B., Kharlashina, N.N., 1995. The use of heat capacity data to calculate carbon isotope fractionation between graphite, diamond, and carbon dioxide: a new approach. Geochim. Cosmochim. Acta 59, 2561–2572.
Pöter, B., Gottschalk, M., Heinrich, W., 2004. Experimental determination of the ammonium partitioning among muscovite, K-feldspar, and aqueous chloride solutions. Lithos 74, 67–90.
Poulsen, M.D., 2022. Controls on Element Exchange during Plumasite-Type Corundum Formation in Ultramafic Rocks: Field Evidence, Geochemical Analyses, and Thermodynamic Modelling on Corundum from Greenland. Department of Geosciences and Natural Resource Management, University of Copenhagen, p. 296.
Ramírez-Salazar, A., Müller, T., Piazolo, S., Webb, A.A.G., Hauzenberger, C., Zuo, J., Haproff, P., Harvey, J., Wong, T.K., Charlton, C., 2021. Tectonics of the Isua supracrustal belt 1: P-T-X-d constraints of a poly-metamorphic terrane. Tectonics 40 (3) e2020TC006516.
Robb, L., 2005. Introduction to Ore-Forming Processes. Wiley Blackwell.
Rosenfeld, J.K., 1979. Ammonium adsorption in nearshore anoxic sediments. Limnol. Oceanogr. 24, 356–364.
Rosing, M.T., 1999. $^{13}$C-depleted carbon microparticles in > 3700-Ma Sea-floor sedimentary rocks from West Greenland. Science 283, 674–676.
Rosing-Schow, N., Bagas, L., Kolb, J., Balić-Žunić, T., Korte, C., Fiorentini, M.L., 2017. Hydrothermal flake graphite mineralisation in Paleoproterozoic rocks of south-East Greenland. Mineral. Deposita 52, 769–789.
Schroeder, P.A., McLain, A.A., 1998. Illite-smectites and the influence of burial diagenesis on the geochemical cycling of nitrogen. Clay Miner. 33, 539–546.
Strauss, H., Moore, T.B., 1992. Abundances and isotopic compositions of carbon and sulfur species in whole rock and kerogen samples. In: Schopf, J.W., Klein, C. (Eds.), The Proterozoic Biosphere - a Multidisciplinary Study. Cambridge University Press, Cambridge, pp. 709–798.
Stüeken, E.E., 2016. Nitrogen in ancient mud: a biosignature? Astrobiology 16, 730–735.
Stüeken, E.E., Zaloumis, J., Meixnerová, J., Buick, R., 2017. Differential metamorphic effects on nitrogen isotopes in kerogen extracts and bulk rocks. Geochim. Cosmochim. Acta 217, 80–94.
Stüeken, E.E., Boocock, T., Szilas, K., Mikhail, S., Gardiner, N.J., 2021. Reconstructing nitrogen sources to Earth's earliest biosphere at 3.7 Ga. Front. Earth Sci. https://doi.org/10.3389/feart.2021.675726.
Tashiro, T., Ishida, A., Hori, M., Igisu, M., Koike, M., Méjean, P., Takahata, N., Sano, Y., Komiya, T., 2017. Early trace of life from 3.95 Ga sedimentary rocks in Labrador, Canada. Nature 549, 516–518.
Ueda, H., Shibuya, T., Sawaki, Y., Saitoh, M., Takai, K., Maruyama, S., 2016. Reactions between komatiite and CO2-rich seawater at 250 and 350 C, 500 bars: implications for hydrogen generation in the Hadean seafloor hydrothermal system. Progr. Earth Planet. Sci. 3, 1–14.
Van Hinsberg, V., Poulsen, M., 2018. Field report - investigations of the metamorhic rocks in the Tasiilaq area, South-East Greenland (SEGMENT-project). Danmarks Grønlands Geol. Undersøgel. Rapport, GEUS 42. https://doi.org/10.22008/gpub/32538.
Wetzel, L.R., Shock, E.L., 2000. Distinguishing ultramafic-from basalt-hosted submarine hydrothermal systems by comparing calculated vent fluid compositions. J. Geophys. Res. Solid Earth 105, 8319–8340.
Whitehouse, M.J., Dunkley, D.J., Kusiak, M.A., Wilde, S.A., 2019. On the true antiquity of Eoarchean chemofossils–assessing the claim for Earth's oldest biogenic graphite in the Saglek Block of Labrador. Precambrian Res. 323, 70–81.
Wille, M., Nebel, O., Van Kranendonk, M.J., Schoenberg, R., Kleinhanns, I.C., Ellwood, M.J., 2013. Mo-Cr-isotope evidence or a reducing Archean atmosphere in 3.46-2.76 Ga black shales from the Pilbara, Western Australia. Chem. Geol. 340, 68–76.
Wright, A.E., Tarney, J., Palmer, K.F., Moorlock, B.S.P., Skinner, A.C., 1973. In: Uo, Keele (Ed.), The Geology of the Angmag Area EG and Possible Relationships to the Lewisian of Scotland.
van Zuilen, M.A., Lepland, A., Arrhenius, G., 2002. Reassessing the evidence for the earliest traces of life. Nature 418, 627–630.
van Zuilen, M.A., Mathew, K., Wopenka, B., Lepland, A., Marti, K., Arrhenius, G., 2005. Nitrogen and argon isotopic signatures in graphite from the 3.8-Ga-old Isua Supracrustal Belt, Southern West Greenland. Geochim. Cosmochim. Acta 69, 1241–1252.